

## Review

# Luminescent metal nanoclusters: controlled synthesis and functional applications

Hong-Tao Sun<sup>1</sup> and Yoshio Sakka<sup>2</sup>

<sup>1</sup> College of Chemistry, Chemical Engineering and Materials Science, Soochow University, Suzhou 215123, People's Republic of China

<sup>2</sup> Advanced Ceramics Group, Materials Processing Unit, National Institute for Materials Science (NIMS), 1-2-1 Sengen, Tsukuba-city, Ibaraki 305-0047, Japan

E-mail: [timothyhsun@gmail.com](mailto:timothyhsun@gmail.com)

Received 24 August 2013

Accepted for publication 17 November 2013

Published 20 December 2013

## Abstract


Luminescent metal nanoclusters that consist of only several, to tens of, metal atoms and which possess sizes comparable to the Fermi wavelength of electrons have recently attracted significant attention. This new class of luminescent materials not only provides the missing link between atomic and nanoparticle behaviors in metals but also they present abundant novel information for the development of new applicable material systems to meet urgent needs in many areas (such as ultrasensitive sensors for heavy metals, bioimaging, as well as information technology) mainly because of their attractive characteristics, including ultra-small size, good dispersibility, excellent biocompatibility and photostability. In this review, we summarize recent advances in the controlled synthesis and application of luminescent metal nanoclusters, with a particular emphasis on Pt, Mo, Bi and alloy clusters. We also speculate on their future and discuss potential developments for their use in sensors, bioimaging and energy harvesting and conversion.

Keywords: nanoclusters, nanoparticles, nanomaterials, metal, bismuth, luminescence, sensors, bioimaging

## 1. Introduction

Current research that tends to shrink the dimensions of materials are driven by the desire to access the unique material properties and performance advantages that occur in the transition to nanometer length scales [1]. Among nanomaterials, the study of metal nanoparticles has a long history in terms of preparation, characterization and applications. Understanding the properties of noble metal nanoparticles and exploring their application potential are major driving forces behind the synthesis of a large variety of nanomaterials [2]. Nanoscale metals are roughly classified into three size domains: large nanoparticles, small nanoparticles and nanoclusters (NCs), corresponding to their

characteristic length scales [3–5]. When the particle size is comparable to, or even larger than, the wavelength of photons that interact with it, the optical responses of these large metal nanoparticles to external electromagnetic fields are simply dependent on their sizes, free-electron density and their nearly bulk-like dielectric function relative to that of the surrounding medium; therefore, they can be quantitatively described with the Mie theory [3, 5]. When the particle size approaches the electron mean free path (~50 nm for Au) [3, 5], the dielectric function and refractive indices become strongly size-dependent [2, 3, 5]. Generally, these two classes of metal nanostructures possess diameters larger than 2 nm. The third kind of particles have sizes comparable with the Fermi wavelength of an electron. The optical, electronic and chemical properties demonstrate large differences with respect to those in the other two size regimes. Nowadays, it is widely accepted that the particles with diameters larger than 2 nm are called nanoparticles, particles smaller

 Content from this work may be used under the terms of the [Creative Commons Attribution-NonCommercial-ShareAlike 3.0 licence](https://creativecommons.org/licenses/by-nc-sa/3.0/). Any further distribution of this work must maintain attribution to the author(s) and the title of the work, journal citation and DOI.

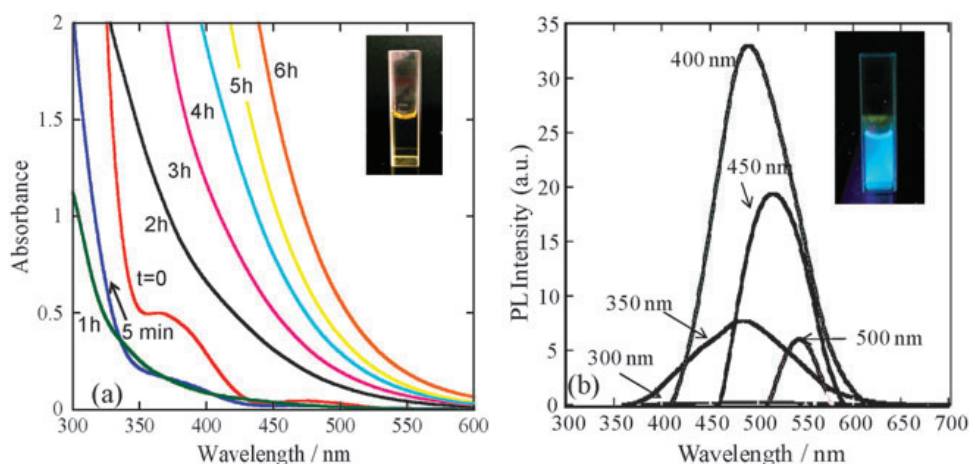


**Figure 1.** (a) UV–Vis spectra at different reaction times of  $t = 0$  ( $\text{H}_2\text{PtCl}_6$ ), 5 min, 1, 2, 3, 4, 5 and 6 h. (b) PL spectra of DMF-protected Pt NCs. Emission spectra for excitation at 300, 350, 400, 450 and 500 nm are shown. The inset photographs show Pt NCs under: (a) room light; and (b) 365 nm UV light. (Reprinted with permission from [39], The Royal Society of Chemistry © 2010.)

than 2 and 1 nm are generally called NCs and sub-NCs, respectively [6, 7]. In view of the similarity between NCs and sub-NCs in many regards (such as preparation approaches, structural features and luminescent behaviors), hereafter we will refer to clusters with sizes smaller than 2 nm as NCs. What is particularly attractive is that such molecule-like metal NCs, composed of a few to roughly a hundred atoms, usually show high-yield photoluminescence (PL), good photostability, large Stokes shift and high emission rates. In the early stage of the study of luminescent noble metal clusters, the photophysical behaviors were roughly predicted by the free-electron model, suggesting that the emission originates from intraband transitions of free electrons. In recent years, employing state-of-the-art quantum chemistry codes, relatively accurate prediction and explanation of the optical properties of a broad range of NCs have been realized [8–12]. A broad range of luminescent metal NCs composed of gold (Au) [5–7, 13–27], silver (Ag) [12, 25–36], copper (Cu) [25, 35, 37, 38], platinum (Pt) [25, 39, 40], bismuth (Bi) [11, 41–45], molybdenum (Mo) [46–48] or mixed metals [49–51] have been successfully fabricated using diverse top-down or bottom-up approaches. Compared with other counterparts, Au and Ag NCs have attracted more attention and have been intensively studied over the past decade. In addition, functional applications in the areas of sensors and bioimaging have been demonstrated. For specialized information on the properties and applications of Au and Ag NCs, the reader is referred to several recent excellent reviews [5–7, 9, 31, 52, 53].

In this review, we focus on luminescent NCs composed of Pt, Mo, Bi and even more than one metal element and will compare their respective advantages and disadvantages. Given that the preparation approaches are strongly dependent on the cluster's type (i.e. one synthesis method for one kind of NCs may not be suitable for others), we summarize the preparation methods and properties of typical NCs according to their compositions. We will then describe the representative achievements regarding their prospective applications in sensors and bioimaging. Finally, we will discuss some of

the key scientific challenges that researchers currently face and present our perspectives on future research trends in this exciting field of science.

## 2. Synthesis approaches for Pt, Mo, Bi and alloy NCs

### 2.1. Pt NCs

Pt is one of the most important metals in catalysis applications. Recent work has shown that  $\text{Pt}_{8-10}$  NCs stabilized on high-surface-area solid supports are 40–100 times more active for the oxidative dehydrogenation of propane than the previously studied Pt catalysts, which is believed to result from the surprisingly high surface reactivity of Pt NCs [54]. In addition to the peculiar catalysis properties of Pt NCs, Kawasaki *et al* [39] were the first to report that Pt NCs synthesized in *N,N*-dimethylformamide (DMF) solution display bright luminescence. Inspired by a DMF reduction method for Au clusters [15], Kawasaki *et al* adopted this technique for Pt NCs by strictly controlling the temperature and stirring speed. In brief, a solution of 150 ml of 0.1 M aqueous  $\text{H}_2\text{PtCl}_6$  was added to 15 ml of DMF that had been preheated to 140 °C. The DMF solution was then refluxed in a 140 °C oil bath with vigorous stirring for 8 h in air [39]. As the reaction proceeded, the solution slowly changed in color, from light yellow to colorless over 0–1 h and, finally, to yellow by 2–6 h. The color changes can be easily monitored by eye or by UV–visible (UV–Vis) absorption spectroscopy (figure 1(a)). The reaction was nearly complete at about 8 h, and the resulting DMF solution of Pt NCs were found to be stable for at least 6 months when stored in the dark, neither precipitating nor changing in spectral properties. The photophysical properties of the as-synthesized NCs are particularly interesting. As shown in figure 1(b), their emission maximum depends on the excitation wavelength (figure 1(b)). Under UV excitation at 350 nm, the maximum emission wavelength is 484 nm. With visible excitation at 500 nm, the maximum emission wavelength is 544 nm. The PL of metal clusters generally

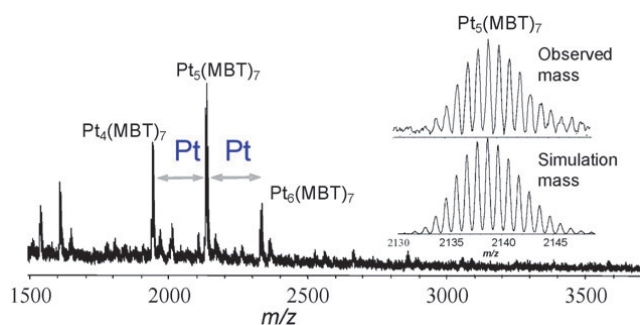


**Figure 2.** MALDI mass spectrum of MBT-protected Pt NCs in the negative ion mode, obtained for DMF-protected Pt NCs by ligand exchange with MBT. (Reprinted with permission from [39], The Royal Society of Chemistry © 2010.)

shifts to short wavelengths as the cluster size decreases. The PL results of Pt NCs suggest that there should be more than one emitter in the sample or the emission originates from the electronic transitions from multiple excited states to the ground state. X-ray photoelectron spectroscopy (XPS) analysis of the dried Pt NCs revealed a peak indicative of Pt  $4f_{7/2}$  at 72.8 eV, suggesting the presence of Pt NCs in a more reduced state rather than Pt compounds in a high valence, such as Pt(II)Cl $_4^{2-}$  (74.4 eV). Given the size of the NCs, the medium binding energy of Pt  $4f_{7/2}$  originates from the Pt at the surface and in the core. Owing to the limited information available [39], much effort is required to further elucidate the luminescent mechanism from these Pt NCs. This approach provides a novel route for preparing highly fluorescent Pt NCs. In particular, this approach combines the advantages of a facile, surfactant-free synthesis that has high variability in the introduction of functionalized ligands and good control over the cluster stability and physical properties [15, 39]. Obviously, the dilute solution of H $_2$ PtCl $_6$  in DMF can be progressively reduced at high temperatures to form Pt atomic clusters, where no further stabilizing agent (such as surfactant, polymer or thiolate-organic compounds) is needed. Thus, DMF is expected to be a weak reducing agent as well as stabilizing ligand for Pt NCs. Furthermore, matrix-assisted laser desorption/ionization mass spectrometry (MALDI-MS) was taken to gather more information of such luminescent Pt clusters after undergoing ligand exchange with 2-mercapto-benzothiazole (MBT). The MALDI-MS spectrum demonstrates the existence of sub-nanometer-sized Pt NCs of 4–6 Pt atoms, using MBT as a novel matrix (figure 2). The mass of the dominant molecular ion observed in negative ion mode was consistent with Pt $_5$ (MBT) $_7$  NCs, the simulated mass obtained in isotropic pattern analysis. This result indicates that the excitation-wavelength dependent emission stems from more than one Pt NC.

Generally, the reduction of metal ions in aqueous solutions results in large nanoparticles instead of small NCs due to their tendency to aggregate. In the case of DMF reduction approach, the stabilizing agent is DMF, which can easily be exchanged with other ligands for functionalization. Additionally, it has been found that the nature of the ligands used for capping the particle surface can markedly affect their emission properties [55]. Therefore,

choosing suitable agents capable of stabilizing clusters from aggregating and enhancing their fluorescence is of vital importance for obtaining small, highly fluorescent metal NCs [7]. Because of the capability of sequestering metal ions from solution, dendrimers have been utilized as templates to prepare luminescent Pt NCs, as first reported by Tanaka *et al* [40]. In brief, Pt NCs were prepared by reducing H $_2$ PtCl $_6$  (6.0 ml, 0.5 M) with NaBH $_4$  (3.0 mmol) in the presence of the fourth-generation polyamidoamine dendrimer (PAMAM (G4-OH)) (0.5 mmol, 71.4 mg). NaBH $_4$  was slowly added to the mixture under continuous stirring. To complete the reaction, the mixture was stirred for 2 weeks. Large Pt colloidal nanoparticles were removed by ultracentrifugation for 30 min at 4 °C. The supernatant emitted a strong blue fluorescence under UV light (365 nm) irradiation, indicating the formation of Pt NCs.

Recently, Yuan and co-workers reported a simple and scalable method for the synthesis of highly fluorescent Pt NCs based on a mild etching environment that was made possible by phase transfer through electrostatic interactions [25]. A simple and fast phase transfer cycle has been developed to process originally polydisperse, nonfluorescent and unstable NCs into monodisperse, highly fluorescent and extremely stable NCs in the same phase (aqueous) and protected by the same thiol ligand. Basically, this method consists of three steps. First, original metal NCs in the aqueous phase were synthesized in the aqueous stock solutions of metal precursors with concentrations of 20 mM and aqueous solutions of thiol ligands. The second step is the transfer of the glutathione-protected metal NCs to an organic phase through the electrostatic interaction ((CTA) $^+$ (COO) $^-$ ) between negatively charged carboxyl groups on the metal NC surface and the positively charged cation of a hydrophobic salt, cetyltrimethylammonium bromide (figure 3) [25]. This phase transfer takes place quickly upon mixing of the reagents. One of the most attractive features of this method is that the fluorescent metal NCs in the organic phase can easily be shuttled back to the aqueous phase. In the third step, upon the addition of hydrophobic salt in chloroform, tetramethylammonium decanoate, to the fluorescent metal NCs in toluene, the hydrophobic decanoate anion D $^-$  quickly forms a hydrophobic salt (CTA) $^+$ D $^-$  with the hydrophobic cation CTA $^+$  on the glutathione-protected metal NCs. The removal of the hydrophobic cation CTA $^+$  from the glutathione-protected metal NCs restores the negative charge on the metal NCs, enabling them to return back to the aqueous phase [25]. As a consequence of the smart design of the chemical reaction, a fast and complete transfer of the fluorescent metal NCs from the organic to the aqueous phase was made possible. Note that the resulting NCs are different from those after the first step in many regards, such as dispersibility, stability and optical properties. This synthetic protocol can be applicable for the synthesis of other classes of highly fluorescent NCs, such as Au, Ag and Cu NCs.

## 2.2. Mo NCs

A Mo element can form fascinating polynuclear structural units. Among these, compounds known as the Chevrel

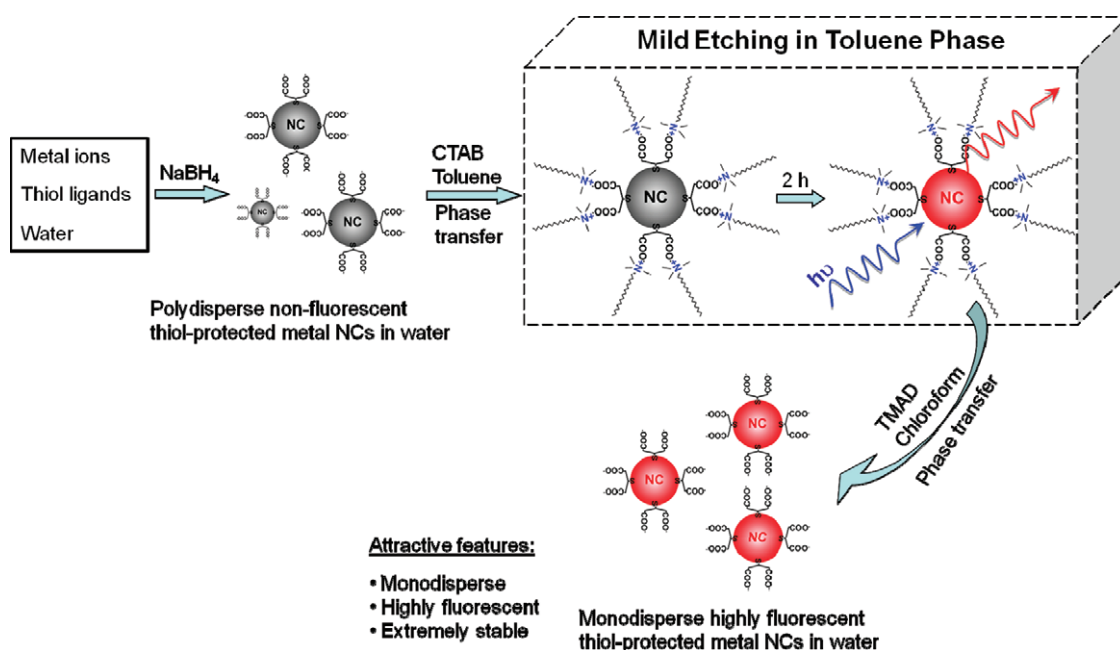


**Figure 3.** A schematic illustration of the process to generate highly fluorescent metal NCs by a phase transfer cycle. (Reprinted with permission from [25], The American Chemical Society © 2011.)

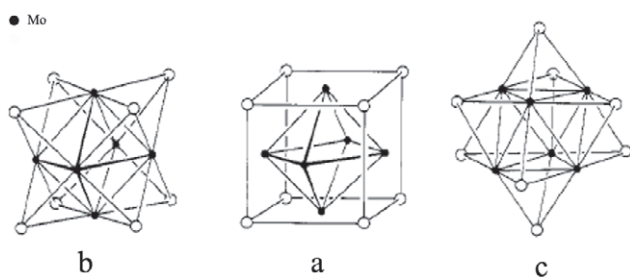


**Figure 4.** The structure of  $\text{Mo}_6\text{X}_8$  (X is S, Se or Te). (Reprinted with permission from [56], The American Chemical Society © 1983.)

phases have been actively studied because they are type II superconductors with relatively high critical fields [56]. Such materials are generally synthesized by high temperature ( $1100^\circ\text{C}$ ) reactions of the chalcogen and Mo metal. Most of these materials can be described by the formula  $\text{MMo}_6\text{X}_8$ , where  $\text{M} = \text{Pb}, \text{Sn}, \text{Ba}, \text{Au}, \text{Cu}, \text{Li}$ , etc and X is usually S, Se or Te [56]. Structurally related, soluble analogues have been prepared; for example,  $\text{Mo}_6\text{S}_8(\text{PEt}_3)_6$  [57]. The fundamental structural unit in the Chevrel phase is the cluster  $\text{Mo}_6\text{X}_8$ , which is shown in three different ways in figure 4. In figure 4(a), an octahedron of Mo atoms ( $\text{Mo-Mo} = 2.7 \text{ \AA}$ ) is encased in a cube of chalcogens ( $\text{Mo-S} 2.45$  or  $\text{Mo-Se} 2.6 \text{ \AA}$ ). Figure 4(b) exhibits the same cluster as consisting of an octahedron with its triangular faces capped by chalcogens, this view emphasizes the connectivity within the cluster. In figure 4(c) the cluster has been reoriented so that a three-fold axis is vertical.

In addition to the stabilization of Mo subnanometer NCs by S, Se or Te in the Chevrel phase, it has well documented that Mo clusters can be well stabilized by halides. Although various reports of the chemistry of the compounds containing Mo have suggested that they were

polynuclear, the first definite structural characterization was a crystallographic study of  $[\text{Mo}_6\text{Cl}_8](\text{OH})_4 \cdot 14\text{H}_2\text{O}$  [58]. The Mo atoms are at the corners of a nearly regular octahedron of edge  $2.63 \text{ \AA}$  while eight chlorine atoms are at the corners of a symmetrically circumscribed cube, such that the shortest Mo-Cl distance is  $2.56 \text{ \AA}$ . Subsequently, Vaughan found that a more complex unit,  $[\text{Mo}_6\text{Cl}_{14}]^{2-}$  ion, exists in  $(\text{NH}_4)_2\text{Mo}_6\text{Cl}_{14} \cdot \text{H}_2\text{O}$  [59]. In idealized cubic symmetry, the  $[\text{Mo}_6\text{Cl}_{14}]^{2-}$  consists of an octahedron of metal atoms surrounded by eight face-bridging and six axial halides. In 1981, Maverick and Gray [60] first investigated the optical properties of  $[\text{Mo}_6\text{Cl}_{14}]^{2-}$  ions and found that they are intensely luminescent. The emission demonstrates a large Stokes shift, the corrected peak wavelength is approximately  $760 \text{ nm}$  (figure 5). Interestingly, the absorption and emission spectra for  $[\text{Mo}_6\text{Cl}_{14}]^{2-}$  in acetonitrile and aqueous HCl solutions at room temperature do not show a large difference. The emission spectra are essentially identical for the two solutions, but they differ in intensity: estimated lower limits for emission quantum yields are 0.04 and 0.005 for the acetonitrile and hydrochloric acids solutions, respectively. Absorption spectra recorded for single crystals of  $(\text{Bu}_4\text{N})_2\text{Mo}_6\text{Cl}_{14}$  reveal weak shoulders at  $530$  and  $590 \text{ nm}$ . Maverick and Gray suggested that the  $590 \text{ nm}$  absorption is associated with the luminescent excited state.

Stimulated by the peculiar electronic properties of Mo clusters, Maverick *et al* further synthesized a series of crystalline compounds containing  $\text{Mo}_6$  clusters. The cluster ions  $\text{Mo}_6\text{Cl}_{14}^{2-}$  and  $\text{Mo}_6\text{Br}_{14}^{2-}$  are luminescent, with emission maxima, lifetimes and quantum yields of  $805, 180 \mu\text{s}$ , and  $0.19$  and  $825, 130 \mu\text{s}$ ,  $0.23$ , respectively, in acetonitrile at room temperature [61]. Since the energies of these bands are similar for  $\text{Mo}_6\text{Cl}_{14}^{2-}$  and  $\text{Mo}_6\text{Br}_{14}^{2-}$ , it is believed that both highest occupied and lowest unoccupied molecular orbitals are largely metal centered [61]. Other researchers



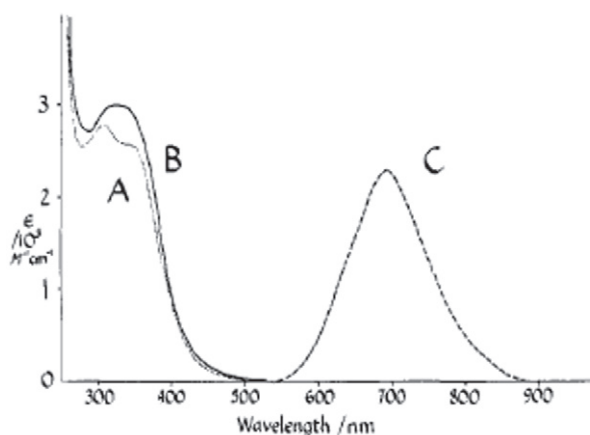


**Figure 5.** Electronic spectra of  $[\text{Mo}_6\text{Cl}_{14}]^{2-}$ . Absorption, (A)  $(\text{NH}_4)_2 - \text{Mo}_6\text{Cl}_{14}$  in 6 M aqueous HCl; (B)  $(\text{Bu}_4\text{N})_2\text{Mo}_6\text{Cl}_{14}$  in  $\text{CH}_3\text{CN}$ . Emission, (C) (arbitrary units). The emission spectrum shown is uncorrected. In the corrected spectrum peak wavelength is at 760 nm. Similar absorption and emission spectra were observed for solid  $(\text{Bu}_4\text{N})_2\text{Mo}_6\text{Cl}_{14}$ . (Reprinted with permission from [60], The American Chemical Society © 1981.)

have revealed that  $\text{Mo}_6$  NCs can be integrated with other material systems, such as semiconducting quantum dots [46], silica [47] and copolymer [48]. In an earlier effort, Grasset *et al* [46] presented the preparation and characterization of a novel organosol and solid state nanocomposite, namely  $((n - \text{C}_4\text{H}_9)_4\text{N})_2\text{Mo}_6\text{Br}_{14}@\text{ZnO}$ , by using an original and simple bottom-up process. The hydrodynamic diameter of these particles is about 12 nm. PL spectroscopy was employed to determine whether the luminescence properties of either the  $\text{Mo}_6$  cluster or the ZnO were affected when the  $\text{Mo}_6\text{Br}_{14}$  cluster core was mixed with the ZnO matrix (figure 6). The steady-state and time-resolved PL results suggest that the emission between 500 and 600 nm stems from the trap state of ZnO, while that over 600 nm are mainly from  $\text{Mo}_6\text{Br}_{14}$  cluster core.

Recently, a simple method to obtain  $\text{Mo}_6$ -PMMA copolymer samples within which  $\text{Mo}_6$  clusters keep their intrinsic luminescence properties has been reported [48]. These emissive properties have been used successfully to sensitize  $\text{Er}^{3+}$  complex emission in the infrared region and within the polymer matrix. Aubert *et al* [47] successfully stabilized the ZnO nanocrystals in the presence of water using polyvinylpyrrolidone for their further coencapsulation along with  $[\text{Mo}_6\text{Br}_{14}]_2$  cluster units in silica to form  $\text{ZnO}-\text{Cs}_2[\text{Mo}_6\text{Br}_{14}]\text{SiO}_2$  nanoparticles using a modified Stöber process. These nanoparticles exhibit tunable emission properties with a broad emission spectrum covering almost the entire visible range for an excitation wavelength of 365 nm (figure 7). Importantly, the luminescence properties remain intact when these nanoparticles are dispersed in water. This advance paves the way for their application as biolabels.

### 2.3. Bi NCs

Bi is one of the most thoroughly investigated main group elements and it exists in a wide array of functional materials such as magnets, superconductors, thermoelectric and

spintronic materials [44]. Basically, depending on the material systems, Bi displays two kinds of structural features. The first case is that Bi exists in functional materials in which it coordinates with other elements. In these compounds, Bi usually demonstrates diverse oxidation states such as +3 and +2. Interestingly, in some compounds such as molecular crystals containing Bi polycations and polyanions Bi can form molecule-like clusters (i.e. Bi coordinates with Bi element itself). The charges that such clusters possess can be balanced by other structural units such as  $[\text{AlCl}_4]^-$  or  $[\text{K-crypt}]^+$  (Crypt = 4,7,13,16,21,24-hexaoxa-1,10-diazabicyclo[8.8.8]hexacosane) [41–45]. Indeed, the study of such peculiar subnanometer Bi NCs dates back to half a century ago. In the 1960s, Smith and co-workers systematically studied the evolution of Bi oxidation states in molten salt systems [62–67]. Based on the thorough examination of spectroscopic properties of Bi-containing liquids, Smith and co-workers first proposed that the absorption bands in UV to near-infrared (NIR) spectral ranges stem from the electronic transitions of subvalent Bi (e.g.  $\text{Bi}^+$ ,  $\text{Bi}_5^{3+}$  or  $\text{Bi}_8^{2+}$ ) [62–67], although the detailed structural information of these subvalent species were not provided. Such pioneering work lead to more concentrated research on the synthesis and characterization of materials containing subvalent Bi in the following decades, and much clearer pictures on the oxidation states of Bi and new synthetic approaches have been reported by Ruck, Kloo and their co-workers [68–74]. These systematic studies suggest that a highly Lewis-acidic environment is a necessary prerequisite for the stabilization of Bi cationic clusters. Ruck *et al* studied the viability of Lewis-acid ionic liquids for the synthesis of low-valent Bi compounds. At room temperature, elemental Bi and Bi (III) cations synproportionate in the ionic liquid  $[\text{BMIM}]\text{Cl}/\text{AlCl}_3$  ( $[\text{BMIM}]^+$ : 1-*n*-butyl-3-methylimidazolium) within minutes. The existence of Bi polycations in the dark colored solution was proven by Raman spectroscopy. Dark-red crystals of  $\text{Bi}_5(\text{AlCl}_4)_3$  were isolated from the ionic liquid [75]. In subsequent studies, Sun *et al* [42] found that  $\text{Bi}_5^{3+}$  and  $\text{Bi}^+$  emitters stabilized by the Lewis acidic liquid show ultrabroad PL with a lifetime of approximately 1  $\mu\text{s}$ . Furthermore, it was found that  $\text{Bi}_5(\text{AlCl}_4)_3$  synthesized by this method exhibits extremely broad NIR PL with a full width at half maximum (FWHM) of >510 nm and an effective PL lifetime of 4.1  $\mu\text{s}$  [41]. This study greatly extends the understanding of photophysical properties of materials containing subvalent Bi, because of the establishment of structure–emitter–property relationships. Indeed, the infrared emission behaviors of material systems containing Bi are rather complicated, and in many cases there is no sound and definitely convincing explanation of emission mechanisms [44]. This work, which uses the molecular crystals as model materials for the study of Bi-related emission mechanisms, represents a new and simple route to gaining deeper understanding of the photophysical behaviors of Bi doped systems. Subsequently, it was found that high-quality  $\text{Bi}_5(\text{AlCl}_4)_3$  crystal prepared by a modified approach displays a broadband emission band from 1 to 2.7  $\mu\text{m}$  [41, 44] (figure 8). Interestingly,  $\text{Bi}_5^{3+}$  in  $\text{Bi}_5(\text{GaCl}_4)_3$  demonstrates a similar emission band under the excitation of

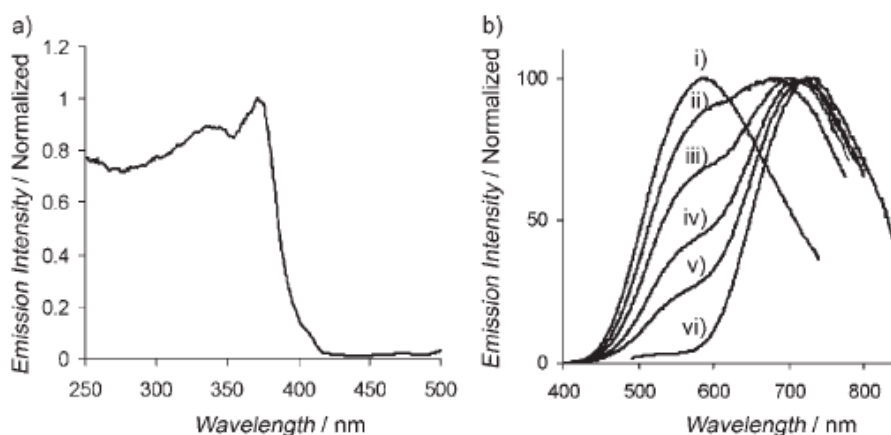


**Figure 6.** (a) Excitation spectrum when monitored at 550 nm. (b) Emission spectra when the excitation wavelengths are at: (i) 380 nm; (ii) 390 nm; (iii) 400 nm; (iv) 405 nm; (v) 410 nm; and (vi) 440 nm. (Reprinted with permission from [46], Wiley-VCH © 2008.)

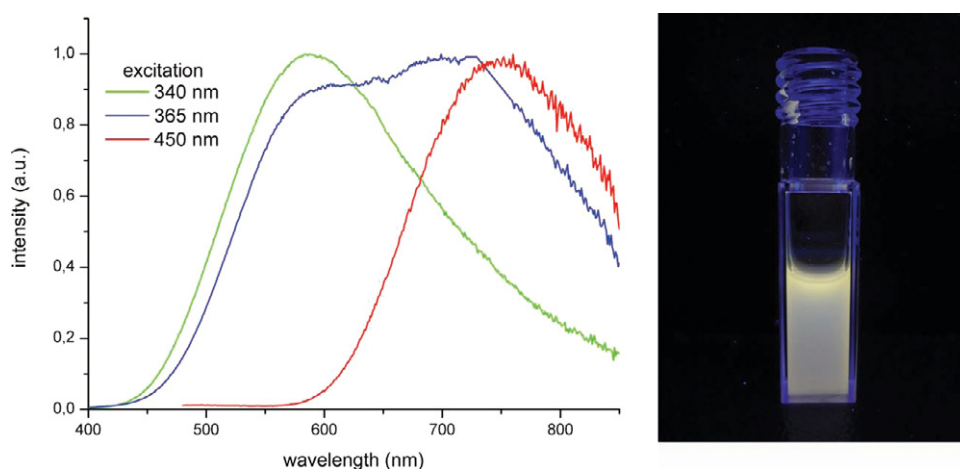


**Figure 7.** Left: normalized emission spectra of ZnO-Cs<sub>2</sub>[Mo<sub>6</sub>Br<sub>14</sub>]@SiO<sub>2</sub> nanoparticles depending on the excitation wavelength. Right: emission of ZnO-Cs<sub>2</sub>[Mo<sub>6</sub>Br<sub>14</sub>]@SiO<sub>2</sub> nanoparticles dispersed in water under 365 nm excitation. (Reprinted with permission from [47], Wiley-VCH © 2013.)

808 nm, although the exact structures of Bi<sub>5</sub><sup>3+</sup> in both crystals are different (figure 8).

In addition to Bi<sub>5</sub><sup>3+</sup>, Sun *et al* [43] experimentally and theoretically studied the photophysical properties of Bi<sub>8</sub><sup>2+</sup> polycation stabilized by [AlCl<sub>4</sub>]<sup>-</sup>. As shown in figure 9(a), the final product, synthesized by a molten salt route, consists of Bi<sub>8</sub>(AlCl<sub>4</sub>)<sub>2</sub> and Bi<sub>5</sub>(AlCl<sub>4</sub>)<sub>3</sub> phases, as evidenced by powder x-ray diffraction (PXRD). It was reported that amorphous red phase, Bi<sub>5</sub>(AlCl<sub>4</sub>)<sub>3</sub>, usually forms when synthesizing Bi<sub>8</sub>(AlCl<sub>4</sub>)<sub>2</sub> crystal [76], which is in good agreement with the PXRD result. However, further detailed microscopic observation revealed that the product is dark black, and lacks a red phase, which suggests that the ratio of Bi<sub>5</sub>(AlCl<sub>4</sub>)<sub>3</sub> to Bi<sub>8</sub>(AlCl<sub>4</sub>)<sub>2</sub> is rather low [43]. The Bi<sub>8</sub>(AlCl<sub>4</sub>)<sub>2</sub> phase consists of Bi<sub>8</sub><sup>2+</sup> polycations and tetrahedral [AlCl<sub>4</sub>]<sup>-</sup> anions (figure 9(b)). The [AlCl<sub>4</sub>]<sup>-</sup> ions render the compounds air- and moisture-sensitive because of the hydrolytic instability of Al-Cl bond.

As displayed in figure 10, four peaks appear at the excitation/emission wavelengths of 290/1180, 490/1180, 636/1187 and 830/1192 nm, among which the intensity of the fourth peak is the strongest [43]. It is obvious that the PL peak

does not display significant excitation-wavelength-dependent shift, which situates it in the range of 1180–1200 nm under different excitation wavelengths. Further detailed analyses suggest that Bi<sub>8</sub><sup>2+</sup> polycations contribute to emission peaking at about 1180 nm, while the emission tails at longer wavelengths results from Bi<sub>5</sub><sup>3+</sup> [43]. This work further evidences that Bi polycations can be smart emitters, whose emission can cover important telecommunication wavelengths.

In addition to molecular crystals containing Bi polycations, it is noteworthy that many compounds with Bi polyanions absorb light in the visible range of the electromagnetic spectrum since they are colored, thus giving promise for unique optical properties [45]. In 2012, Sun and coworkers first reported that a single crystal of (K-crypt)<sub>2</sub>Bi<sub>2</sub> which contains [Bi<sub>2</sub>]<sup>2-</sup> polyanions displays ultrabroad NIR emission at around 1190 nm (figure 11). As demonstrated in figure 11(b), the emission spectrum under 641 nm excitation has a very broad emission range, spanning from 975 to 1400 nm [45]. The full width at half maximum (FWHM) of the spectrum is 212 nm and the emission peak is around 1190 nm. The emission spectrum by Gaussian

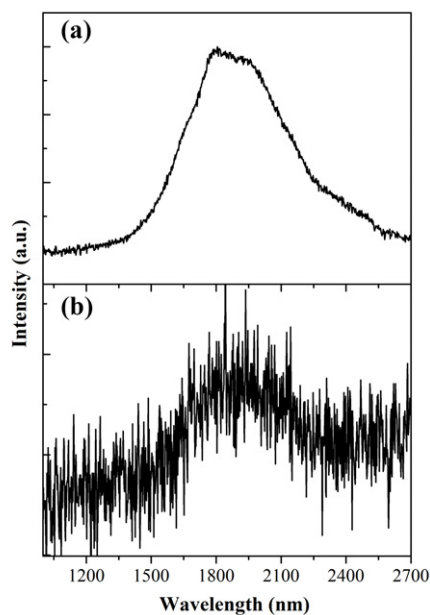


**Figure 8.** PL spectra of  $\text{Bi}_5(\text{AlCl}_4)_3$  (a) and  $\text{Bi}_5(\text{GaCl}_4)_3$  (b) samples under 808 nm excitation. (Reproduced with permission from [44], The Royal Society of Chemistry © 2012.)

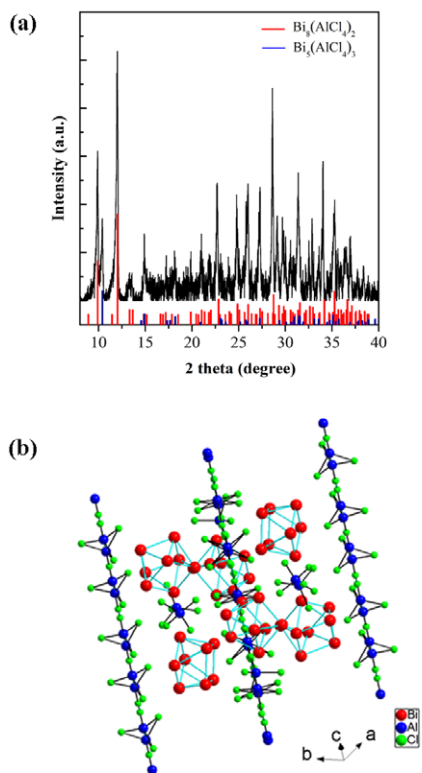


**Figure 9.** (a) PXRD of the synthesized product after removal of the background. The vertical red and blue lines represent the diffraction peaks of  $\text{Bi}_8(\text{AlCl}_4)_2$  (CSD no: 405159) and  $\text{Bi}_5(\text{AlCl}_4)_3$  (CSD no: 420082) phases, respectively. (b) A general view of the structure of  $\text{Bi}_8(\text{AlCl}_4)_2$ . (Reproduced with permission from [43], The Royal Society of Chemistry © 2012.)

fitting yields three components peaking at 1047, 1190 and 1331 nm with FWHMs of 99, 146 and 56 nm, respectively (figure 11(b)), whose emission energies are lower than the corresponding absorption energies at 990, 1090 and 1273 nm,

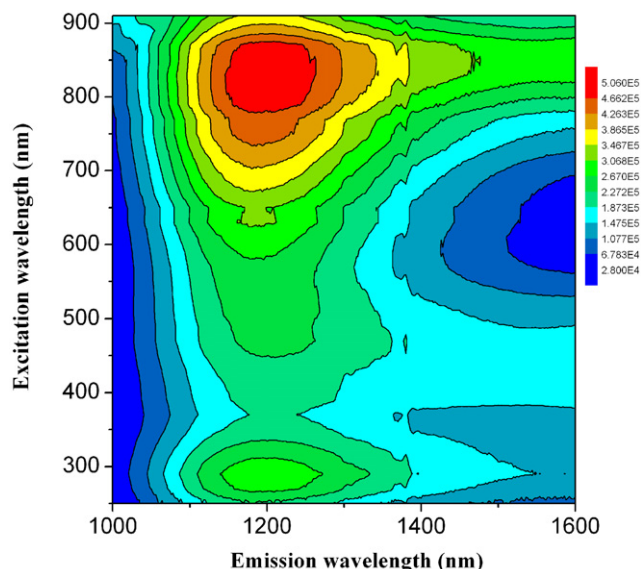


**Figure 10.** Contour excitation-emission matrix plot of the obtained sample. Note that the jump at around 1400 nm results from measurement artifacts. (Reproduced with permission from [43], The Royal Society of Chemistry © 2012.)

respectively [45]. A qualitative explanation of the observed photophysical behavior is proposed [45]. The  $[\text{Bi}_2]^{2-}$  anion absorbs photons with energies in the NIR and visible ranges. After irradiation with high-energy photons, the electrons in the upper excited levels tend to nonradiatively relax to the first three excited levels from where the NIR emissions take place. That is, NIR PL results from the radiative electronic transitions from the first three excited levels to the ground level based on a one-photon process. The overlap of the three emission bands leads to the observed ultrabroad PL band ranging from 975 to 1400 nm. This result greatly deepens the understanding of Bi-related NIR emission behavior and leads to a reconsideration of the fundamentally important issue on Bi-related PL mechanisms in some material systems, such as bulk glasses, fibers and conventional optical crystals [45].

Additionally, the analysis of high-resolution synchrotron PXRD data coupled with steady-state and time-resolved PL spectra and time-dependent density functional theory (TDDFT) has found that the substructures of  $\text{Bi}^+$  residing in the sodalite cages of zeolites Y result in ultrabroad and tunable NIR PL [11]. Subsequently, the structural and photophysical features of the resulting zeolite Y have been thoroughly characterized by using extensive experimental techniques, including nuclear magnetic resonance, electron paramagnetic resonance, two-dimensional excitation-emission and absorption spectra [77]. A thorough analysis of luminescence and absorption spectra, coupled with TDDFT calculations, suggests that all  $\text{Bi}^+$  substructures (i.e.  $\text{Bi}_4^{4+}$ ,  $\text{Bi}_3^{3+}$ ,  $\text{Bi}_2^{2+}$  and  $\text{Bi}^+$ ) are optically active in the NIR spectral range. It is found that  $\text{Bi}^+$ ,  $\text{Bi}_2^{2+}$ ,  $\text{Bi}_3^{3+}$  and  $\text{Bi}_4^{4+}$  units result in NIR emissions peaking at about 1050, 1135, 1145, 1240/1285 nm, respectively [77]. This finding represents an important contribution to the understanding of the processes involved in the formation of  $\text{Bi}^+$  and of the luminescence mechanisms of  $\text{Bi}^+$  substructures.



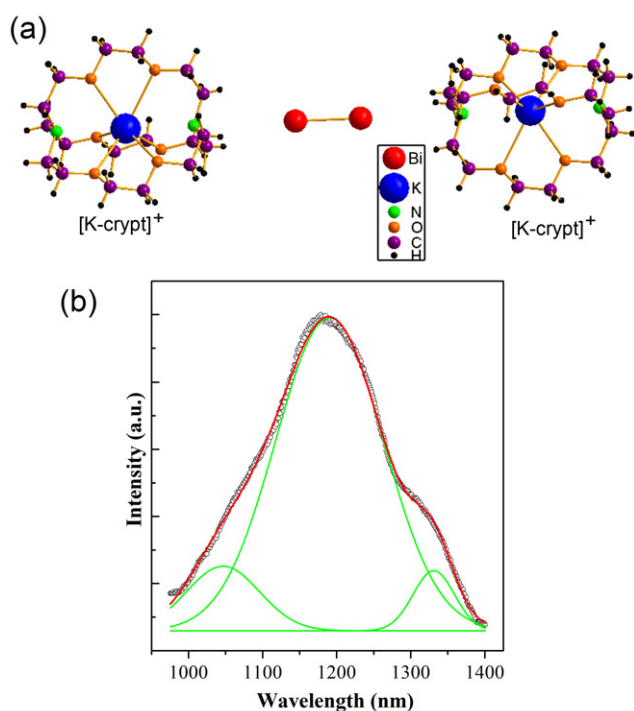


**Figure 11.** (a) Part of the structure of  $(\text{K-crypt})_2\text{Bi}_2$ . (b) The PL spectrum of  $(\text{K-crypt})_2\text{Bi}_2$  crystals under 641 nm excitation light. The black, red and green curves are experimental, fitted and three decomposed Gaussian peaks, respectively. (Reproduced with permission from [45], The Royal Society of Chemistry © 2012.)

The dominant advantage of Bi NCs lies in their attractive infrared emission feature, which might lead to a broad range of applications in bioimaging, telecommunications and lasers. However, such NCs can only be stabilized by air-sensitive units or templates that can absorb water, resulting in the air instability of the final product. Furthermore, these NCs generally exist in crystalline matrices. It is greatly expected that monodisperse Bi NCs can be obtained for their practical applications. With enough effort in these directions, it is hopeful that air-stable, monodisperse and highly luminescent Bi NCs can be synthesized.

#### 2.4. Alloy metal NCs

Atomically precise molecules of noble metals, such as Au, Ag, Pt and Cu with quantum confinement phenomena, have been some of the most fascinating materials in molecular cluster science during recent years [5, 7, 9]. However, because PL from such NCs generally occurs only at some specific spectral ranges, the ability to tune these optoelectronic behaviors has been limited. Since the photophysical properties of NCs are closely correlated with their compositions and structures, there remains the possibility of manipulating their properties through precise variations in composition [50]. This has stimulated the exploration of luminescent alloy NCs. A recent example of manipulation in alloy compositions is the creation of stable 13-atom AuAg alloy clusters [49] (figure 12). These alloy NCs are prepared from the  $\text{Ag}_{7,8}$  cluster (a mixture containing  $\text{Ag}_7$  and  $\text{Ag}_8$  NCs). Basically, synthesis of AuAg alloy NCs involves three steps. The

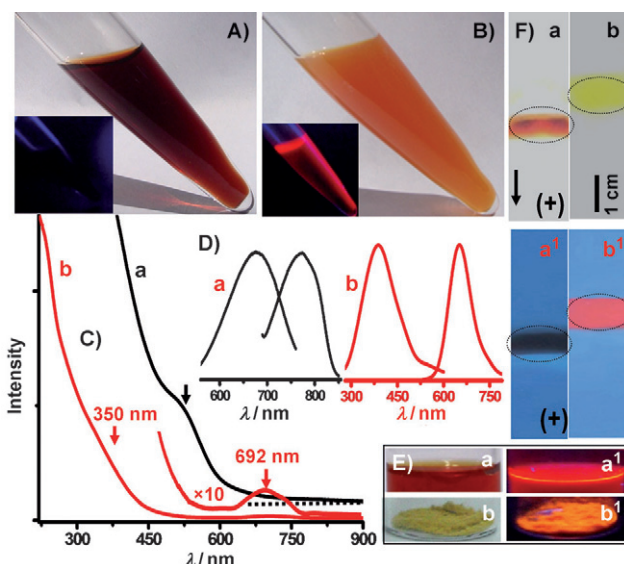


**Figure 12.** Changes observed during synthesis. (A,B) Solutions of  $\text{Ag}_{7,8}$  (A) and the alloy NC (B) after synthesis under visible light. Insets: the same samples under UV light. (C) UV-Vis profile of (a)  $\text{Ag}_{7,8}$  and (b) Alloy NC measured in water; arrows indicate the well-defined optical features of the cluster. (D) Luminescence spectra of (a)  $\text{Ag}_{7,8}$  and (b) alloy NC in water at 300 K. (E) Photographs of (a, a<sup>1</sup>) alloy NC in water and (b, b<sup>1</sup>) in the solid state under visible and UV light. (F) Comparison of the polyacrylamide gel electrophoresis results of (a, a<sup>1</sup>)  $\text{Ag}_8$  and (b, b<sup>1</sup>) alloy NC. Photographs of gel in visible (a, b) and UV (a<sup>1</sup>, b<sup>1</sup>) light. Band positions are marked with circles on the gels. (Reproduced with permission from [49], Wiley-VCH © 2012.)

first step is the synthesis of polydisperse  $\text{Ag}@H_2\text{MSA}$  nanoparticles followed by the synthesis of  $\text{Ag}_{7,8}$  clusters by interfacial etching in the second step. In the third step, addition of an appropriate amount of 10 mM  $\text{HAuCl}_4$  to the as-synthesized  $\text{Ag}_{7,8}$  cluster yields the alloy cluster.

In a subsequent work, Mohanty *et al* [50] further synthesized a series of alloy NCs with tunable compositions in a bovine serum albumin (BSA) template starting from Au and Ag clusters, either through NC-NC interaction or galvanic exchange reaction. The existence of the alloy is obviously confirmed using elemental analysis by XPS and scanning electron microscopy and energy dispersive spectroscopy (SEM-EDS). The mass spectra of the mixture of clusters show well-defined compositions with complete tenability (figure 13), suggesting the formation of  $\text{Au}_{1-x}\text{Ag}_x$  clusters across the entire compositional window.

In addition to alloy NCs with noble metals, synthesis of luminescent NCs consisting of cheap metals not only presents a route for low-cost applicable materials but also might give rise to new opportunities for the understanding of the formation mechanisms of alloy NCs. In this regard, Andolina *et al* [51] reported the synthesis of discrete, bimetallic Au-Cu NC alloys with diameters of 2–3 nm which display PL that can be tuned by changing the alloy composition. Upon varying the composition of the NCs from 0 to 100% molar ratio Cu, the PL maxima shift from 947 to 1067 nm under the excitation of 360 nm (figure 14). The resulting particles exhibit brightness values that are more than an order of magnitude larger



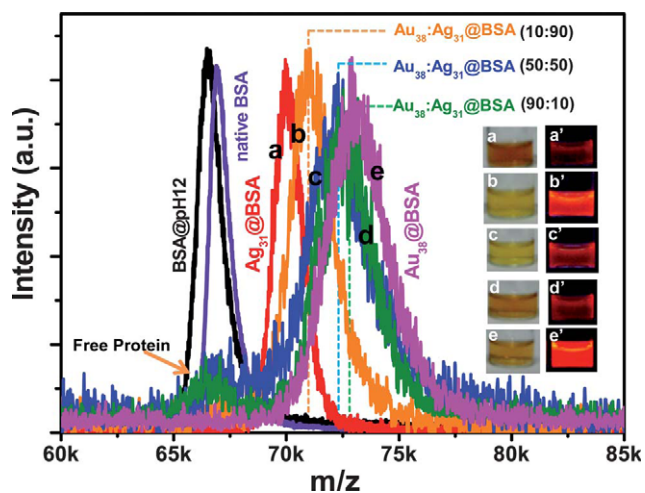


**Figure 13.** MALDI MS data shows the tunability of the composition of the Au–Ag alloy clusters in protein templates. MS of native BSA (violet) and BSA at pH 12 (black). The products of 900 ml  $\text{Ag}_{\text{NC}}@BSA + 100 \mu\text{l Au}_{\text{NC}}@BSA(90:10)$  peak at  $m/z$  71 100 (orange trace), 500 ml  $\text{Ag}_{\text{NC}}@BSA + 500 \mu\text{l Au}_{\text{NC}}@BSA(50:50)$  peak at  $m/z$  72 300 (blue trace) and 100 ml  $\text{Ag}_{\text{NC}}@BSA + 900 \mu\text{l Au}_{\text{NC}}@BSA(10:90)$  peak at  $m/z$  72 800 (olive trace) lie between  $\text{Ag}_{\text{NC}}@BSA$  (red trace) and  $\text{Au}_{\text{NC}}@BSA$  (magenta trace), suggesting compositional variation in the alloys. Inset photographs: (a)  $\text{Ag}_{\text{NC}}@BSA$ ; (b)  $\text{Au}_{\text{NC}}: \text{Ag}_{\text{NC}}@BSA(10:90)$ ; (c) 50:50  $\text{Au}_{\text{NC}}: \text{Ag}_{\text{NC}}$ ; (d)  $\text{Au}_{\text{NC}}: \text{Ag}_{\text{NC}}(90:10)$  and (e)  $\text{Au}_{\text{NC}}@BSA$  under visible light (left) and UV light (right). The ratio mentioned here is v/v, which can also be considered as a molar ratio since Au and Ag solutions of the same molarity were used. (Reproduced with permission from [50], The Royal Society of Chemistry © 2012.)

than the brightest NIR-emitting lanthanide complexes and small-molecule probes evaluated under similar conditions. The PL from these alloy NCs is very intriguing, given that the emission can extend to the NIR spectral range. These novel NCs may become a promising class of stable and tunable NIR nanoprobes that can be readily translated into biological settings if they possess excellent photostability and low cytotoxicity.

Although alloy NCs possess attractive photophysical properties and can be synthesized by well-controlled approaches, there are still a number of scientific issues that require to be answered (such as the detailed coordination environments of metal species in alloys, the long-term physiochemical stability and the exact PL mechanisms of such alloy NCs). These issues will hopefully be solved when using other powerful analytic techniques, such as x-ray crystallography and time-resolved x-ray absorption spectroscopy.

### 3. Functional applications

#### 3.1. Bioimaging

Fluorescence imaging offers unique advantages over other imaging methods in regard to sensitivity, multiplex detection capabilities and equipment cost [7]. Until now, a wide array of novel nanomaterials including quantum dots, organic dyes and dye-doped or undoped inorganic NPs have been developed

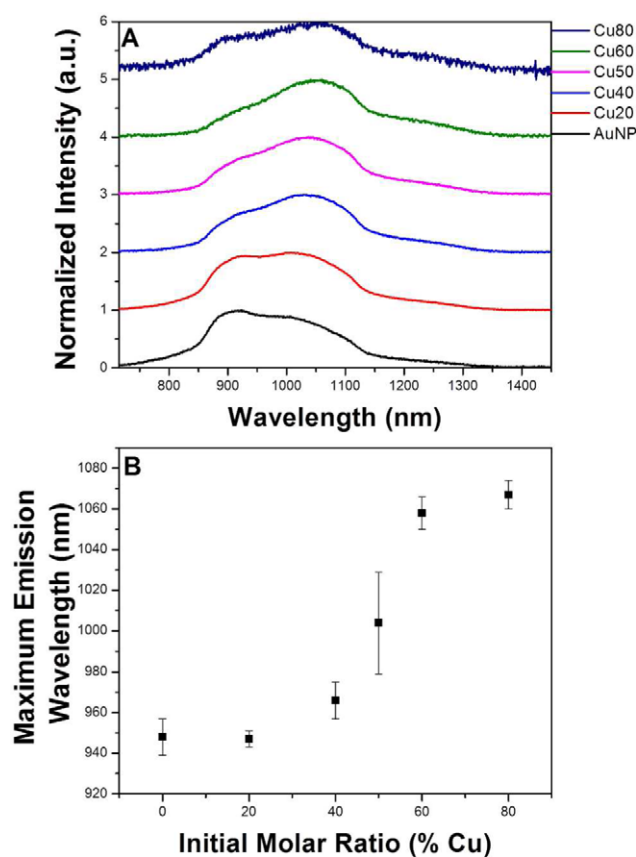


**Figure 14.** (A) Normalized and offset emission spectra of  $\text{Au}_x\text{Cu}_y$  NCs, excitation at 360 nm. (B) Average emission wavelength as a function of the initial molar ratio of Cu. (Reproduced with permission from [51], The American Chemical Society © 2013.)

for bioimaging [78, 79]. For example, quantum dots have been successfully used as *in vivo* cancer-targeted imaging agents of living animals [80]. However, most of quantum dots contain toxic elements (such as cadmium and lead) and organic dyes are easy to be photobleached, which makes them rather difficult for *in vivo* imaging in humans [79]. In contrast, fluorescent metal NCs are smaller and exhibit bright and stable emission, and good biocompatibility, making them attractive alternatives as fluorescent probes for bioimaging. Interestingly, the emission from various metal NCs covers not only the visible spectral range but also the NIR biological window, which implies that NCs are suitable for both cell and *in vivo* imaging.

A number of papers have reported biological imaging applications based on fluorescent metal NCs. Tanaka *et al* [40] investigated the capability of  $\text{Pt}_5$  NCs to act as fluorescent probes for live cell imaging. First, the  $\text{Pt}_5(\text{MAA})_8$  (MAA = mercaptoacetic acid) is conjugated with protein A using a 1-[(3-dimethylamino)-propyl]-3-ethylcarbodiimide hydrochloride/*N*-hydroxysulfosuccinimide coupling reaction. Next,  $\text{Pt}_5(\text{MAA})_8$ -(protein A) is bound to an antichemokine receptor antibody through the Fc moiety of the antibody (figure 15) [40]. After the introduction of  $\text{Pt}_5(\text{MAA})_8$ -(protein A)-(anti-CXCR4-Ab) into HeLa cells, the HeLa cells were incubated for 5 min prior to cell imaging. Figure 16(a) shows a confocal fluorescence

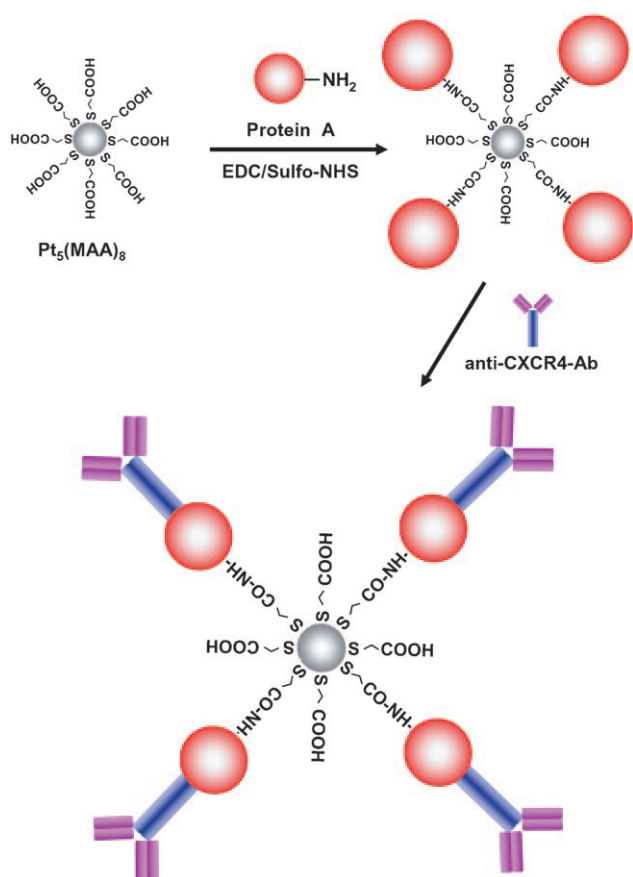


**Figure 15.** Preparation of  $\text{Pt}_5(\text{MAA})_8$ -(protein A)-(anti-CXCR4-Ab). (Reproduced with permission from [40], Wiley-VCH © 2011.)

image of HeLa cells labeled with  $\text{Pt}_5(\text{MAA})_8$  NCs. A blue fluorescence signal was clearly observed on cell membranes and no fluorescence signal was detected in a control sample labeled without  $\text{Pt}_5(\text{MAA})_8$  (figure 16(b)). Interestingly, the resulting NCs demonstrate the specific binding to the chemokine receptor [40]. As shown in figure 16(c), no fluorescence signal was observed, indicating that CHO-K1 cells were not stained by  $\text{Pt}_5(\text{MAA})_8$ . Furthermore, the  $\text{Pt}_5$  NCs display low cytotoxicity [40]. Figure 16(d) shows the viability of cells labeled with three different concentrations of  $\text{Pt}_5$  NCs. After 12 h incubation, more than 89% of the cells were alive and even after 48 h incubation cell viability was still more than 85%. These viabilities were comparable to controls [40]. This suggests that  $\text{Pt}_5$  NCs are harmless fluorescent probes that are applicable for the long-term imaging of living cells.

Recently, Zheng *et al* [22] found that the renal clearance of 2 nm glutathione-coated luminescent Au NCs was more than 10–100 times better than that of similarly sized non-luminescent Au NPs. The small size in combination with surface ligands not only enables the majority of the luminescent Au NCs to be cleared from the body through kidney filtration but also stabilizes the luminescent Au NCs during blood circulation [7, 22]. It is believed that the approach demonstrated by Zheng *et al* might be suitable for the improvement of the biological compatibility of other

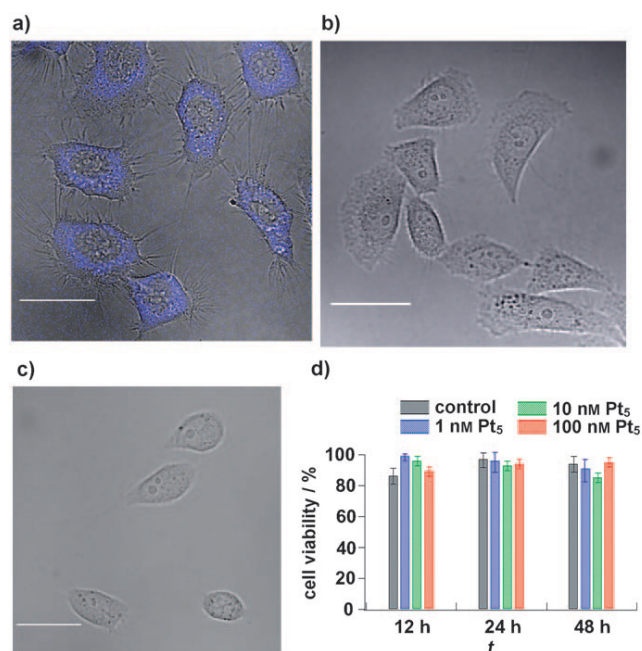


**Figure 16.** Confocal fluorescence microscopic images merged with differential interference contrast (DIC) images of living HeLa cells labeled with (a) and without (b)  $\text{Pt}_5(\text{MAA})_8$ -(protein A)-(anti-CXCR4-Ab). (c) Confocal fluorescence microscopic images merged with DIC images of living CHO-K1 cells in the presence of  $\text{Pt}_5(\text{MAA})_8$ -(protein A)-(anti-CXCR4-Ab). The scale bars are 20  $\mu\text{m}$ . (d) Cell viability of HeLa cells. Cells were incubated with 1, 10 and 100 nm  $\text{Pt}_5$  NCs at 37 °C. The black bars show the cell viability of control samples in the absence of  $\text{Pt}_5$  NCs. (Reproduced with permission from [40], Wiley-VCH © 2011.)

classes of NCs consisting of the element of Pt, Mo or Au/Ag, rendering them promising contrast imaging agents for cell and *in vivo* fluorescence imaging.

### 3.2. Sensors

The ions of heavy metals (such as mercury, lead and cadmium) are highly toxic pollutants to the environment. The accumulation of heavy metal ions in the body through food chains can ultimately induce various diseases [6]. For example,  $\text{Hg}^{2+}$  is a highly toxic and widespread pollutant ion, and its damaging effects to the brain, nervous system and the kidney even at very low concentrations are well known [81]. Ying *et al* [82] demonstrated that BSA-stabilized Au NCs is rather sensitive for the detection of  $\text{Hg}^{2+}$ . The sensing mechanism was based on the quenching of luminescence of Au NCs because of high-affinity metallophilic  $\text{Hg}^{2+}$ - $\text{Au}^+$  interactions (figure 17(a)). Upon adding  $\text{Hg}^{2+}$  ions (50  $\mu\text{M}$ ) to an aqueous Au NCs solution (20  $\mu\text{M}$ ), the red fluorescence of Au NCs was completely quenched within seconds (figure 17(b)). The red fluorescence of Au NCs could be partially recovered by adding a strong reductant (e.g. sodium borohydride) to Au NCs solution in the presence of  $\text{Hg}^{2+}$  ions [82]. Furthermore, BSA-stabilized Au NCs display high specificity toward the detection of  $\text{Hg}^{2+}$  over other environmentally relevant metal ions owing to the high specificity of  $\text{Hg}^{2+}$ - $\text{Au}^+$  interactions. Figure 17(c) shows that

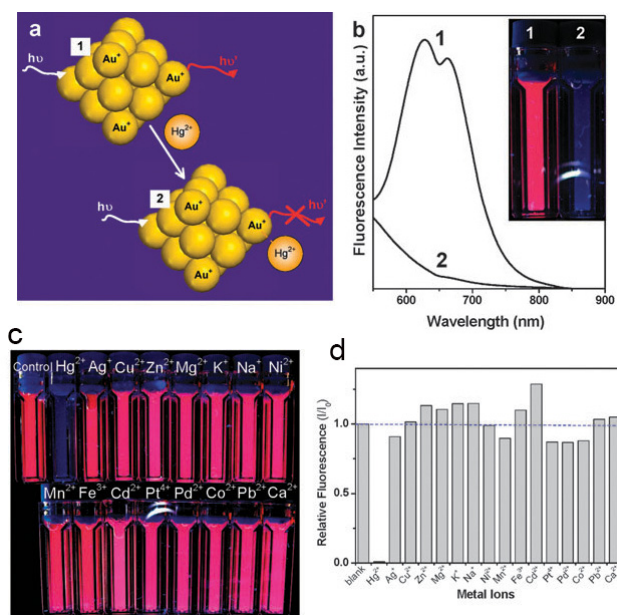


**Figure 17.** (a) Schematic representation of Hg<sup>2+</sup> sensing based on the fluorescence quenching of Au NCs resulting from high-affinity metalphilic Hg<sup>2+</sup>-Au<sup>+</sup> bonds. (b) Photoemission spectra (ex. wavelength is 470 nm) and (inset) photographs under UV light (354 nm) of Au NCs (20 mM) in the (1) absence and (2) presence of Hg<sup>2+</sup> ions (50 mM). (c) Photographs under UV light and (d) relative fluorescence ( $I/I_0$ ) under 470 nm excitation of aqueous Au NC solutions (20 mM) in the presence of 50 mM of various metal ions. (Reproduced with permission from [82], The Royal Society of Chemistry © 2010.)

the fluorescence of Au NCs was not quenched by 50 mM of Ag<sup>+</sup>, Cu<sup>2+</sup>, Zn<sup>2+</sup>, Mg<sup>2+</sup>, K<sup>+</sup>, Na<sup>+</sup>, Ni<sup>2+</sup>, Mn<sup>2+</sup>, Fe<sup>3+</sup>, Cd<sup>2+</sup>, Pt<sup>4+</sup>, Pd<sup>2+</sup>, Co<sup>2+</sup>, Pb<sup>2+</sup> and Ca<sup>2+</sup> ions [82]. Only Hg<sup>2+</sup> ions led to almost 100% quenching of Au NC fluorescence (figure 17(d)). The estimated detection limit for Hg<sup>2+</sup> ions is 0.5 nM, which is much lower than the maximum level of mercury in drinking water (10 nM) permitted by the US Environmental Protection Agency (EPA).

Lead ions (Pb<sup>2+</sup>) are a highly toxic environmental pollutant that can cause damage to the kidney, the liver and the nervous system and pose severe effects on human health [83, 84]. The US EPA sets the maximum contamination level for lead in drinking water at 15  $\mu\text{g l}^{-1}$  or 75 nM. Recently, Yuan *et al* [85] developed a novel strategy to prepare functionalized fluorescent Au NCs based on a modified ligand exchange reaction and demonstrated the capability of glutathione functionalized Au NCs for ultrasensitive and selective Pb<sup>2+</sup> sensing. The relative intensity reduction shows a nice linear relationship with Pb<sup>2+</sup> concentration ranging from 5 nM to 5 mM. The limit of detection is determined to be 2 nM with a signal-to-noise ratio of 3.

The work by Ying *et al* [82] and Yuan *et al* [85] has clearly revealed that luminescent NCs can be exploited as sensors for toxic ions in the environment. It is noted that the functionality of such NCs is closely correlated with the ligands used for their stabilization. Given that the study of luminescent NCs is at the research stage and the more novel systems (e.g. alloy clusters) will be found in the near future,

the employment of NCs as sensors for toxic ions has a bright future. By using environmentally friendly NCs with higher emission yields it is possible to develop more sensitive sensors for various toxic ions.

#### 4. Conclusions and perspective

In this review, we have summarized the recent progress in the controlled synthesis and application of luminescent metal NCs, with a particular emphasis on Pt, Mo, Bi and alloy clusters. Compared with widely studied noble metal NCs, Pt, Mo, Bi and alloy NCs have received relatively less attention, and many works are still at the research stage. The abundant photophysical and physiochemical properties of NCs help researchers in this domain to deepen their understanding of the rationality of synthesis approaches, as well as the inherent interaction mechanisms with other species (e.g. when it is used as a sensor for toxic elements). However, a number of challenges remain in this exciting field of science.

Firstly, more effective synthesis protocols are greatly needed for the synthesis of highly luminescent and well-dispersed Pt, Mo, Bi and alloy clusters. In particular, most of the above-mentioned metal NCs possess a relatively weak brightness in comparison to semiconducting quantum dots and many organic dyes. Furthermore, it is noteworthy that some NCs (such as Mo and Bi NCs) are stable only in suitable matrices. Facing this, it is believed that developing revolutionary approaches for their synthesis is important for their broader application.

Secondly, more work should be done in the near future to establish relationships between the structure and emission properties. It is found that in many cases the resulting NCs are poly-disperse and display broad emission bands. Basically, there are two possibilities for this phenomenon: the emission is either from emitters with one kind of size or from those with diverse sizes. Furthermore, the photophysical properties of NCs are dependent on the protection ligands. To convincingly explain the observed luminescence from NCs, structural analyses of the obtained systems by x-ray crystallography are required, although in many cases it is difficult to culture high-quality single crystals of tiny NCs.

Thirdly, the emission and excitation ranges should be optimized. Most NCs emit in the spectral range <1000 nm. It is anticipated that the spectral range can be further extended into NIR or even mid-infrared, given their potential for both telecommunications and bioimaging. Furthermore, much effort is needed to build optical devices based on such NCs, which might find some commercial applications. Furthermore, most reported NCs have a UV excitation band and large-Stokes shifts occur, resulting in visible or NIR emissions. Indeed, this is not favorable for bioimaging, especially for *in vivo* imaging, owing to the weak penetration of UV light in living tissues. To solve this difficulty, one should develop NCs that exhibit NIR-excitable NIR emission.

In summary, given their low-cost, ready scalability, excellent chemical stability, colloidal stability and photostability, fluorescent metal NCs have shown primary potential in optical imaging and related disciplines. With



further systematic experimental and theoretical studies, it is believed that these NC materials will find broad applications in addressing important issues related to the environment, medicine, diagnosis, telecommunications, and laser science.

## Acknowledgments

HTS thanks the funding support from Soochow University, China and a project funded by the Priority Academic Program Development of Jiangsu Higher Education Institutions. The authors thank corresponding publishers for the kind permissions to reproduce their materials, especially figures, used in this review.

## References

- [1] Grainger D W and Castner D G 2008 *Adv. Mater.* **20** 867
- [2] Sau T K, Rogach A L, Jäckel F, Klar T A and Feldmann C 2010 *Adv. Mater.* **22** 1805
- [3] Kreibig U and Vollmer M 1995 *Optical Properties of Metal Clusters* (Berlin: Springer)
- [4] Ashcroft N W and Mermin N D 1976 *Solid State Physics* (New York: Holt, Rinehart and Winston)
- [5] Zheng J, Nicovich P R and Dickson R M 2007 *Annu. Rev. Phys. Chem.* **58** 409
- [6] Lu Y Z and Chen W 2012 *Chem. Soc. Rev.* **41** 3594
- [7] Shang L, Dong S J and Nienhaus G U 2011 *Nano Today* **6** 401
- [8] Zhu M Z, Aikens C M, Hollander F J, Schatz G C and Jin R C 2008 *J. Am. Chem. Soc.* **130** 5883
- [9] Jin R C 2010 *Nanoscale* **2** 343
- [10] Pei Y, Pal R, Liu C Y, Gao Y, Zhang Z H and Zeng X C 2012 *J. Am. Chem. Soc.* **134** 3015
- [11] Sun H T, Matsushita Y, Sakka Y, Shirahata Y, Tanaka M, Katsuya Y, Gao H and Kobayashi K 2012 *J. Am. Chem. Soc.* **134** 2918
- [12] Bakr O M, Amendola V, Aikens C M, Wenseleers W, Li R, Negro L D, Schatz G C and Stellacci F 2009 *Angew. Chem. Int. Edn Engl.* **48** 5921
- [13] Zheng J, Petty P T and Dickson R M 2003 *J. Am. Chem. Soc.* **125** 7780
- [14] Zheng J, Zhang C W and Dickson R M 2004 *Phys. Rev. Lett.* **93** 077402
- [15] Liu X F, Li C H, Xu J L, Lv J, Zhu M, Guo Y B, Cui S, Liu H B, Wang S and Li Y L 2008 *J. Phys. Chem. C* **112** 10778
- [16] Xie J P, Zheng Y G and Ying J Y 2009 *J. Am. Chem. Soc.* **131** 888
- [17] Yang X, Shi M M, Zhou R J, Chen X Q and Chen H Z 2011 *Nanoscale* **3** 2596
- [18] Sun C J *et al* 2011 *J. Am. Chem. Soc.* **133** 8617
- [19] Huang X, Li B Y, Li L, Zhang H, Majeed I, Hussain I and Tan B N 2012 *J. Phys. Chem. C* **114** 448
- [20] Shang L, Dorlich R M, Brandholt S, Schneider R, Trouillet V, Bruns M, Gerthsen D and Nienhaus G U 2011 *Nanoscale* **3** 2009
- [21] Wang H H *et al* 2011 *ACS Nano* **5** 4337
- [22] Zhou C, Long M, Qin Y P, Sun X K and Zheng J 2011 *Angew. Chem. Int. Edn Engl.* **50** 3168
- [23] Kawasaki H, Hamaguchi K, Osaka I and Arakawa R 2011 *Adv. Funct. Mater.* **21** 3508
- [24] Shang L, Yang L, Stockmar F, Popescu R, Trouillet V, Bruns M, Gerthsen D and Nienhaus G 2012 *Nanoscale* **4** 4155
- [25] Yuan X, Luo Z, Zhang Q, Zhang X, Zheng Y, Lee J and Xie J 2011 *ACS Nano* **5** 8800
- [26] Wang Z J, Wu L N, Cai W and Jiang Z H 2012 *J. Mater. Chem.* **22** 3632
- [27] Wang Z J, Cai W and Sui J H 2009 *ChemPhysChem* **10** 2012
- [28] Kim Y and Seff K 1977 *J. Am. Chem. Soc.* **99** 7055
- [29] Zheng J, Petty P T and Dickson R M 2002 *J. Am. Chem. Soc.* **124** 13982
- [30] Shang L and Dong S J 2008 *Chem. Commun.* **2008** 1088
- [31] Choi S, Dickson R M and Yu J H 2012 *Chem. Soc. Rev.* **41** 1867
- [32] Petty J T, Fan C Y, Story S P, Sengupta B, Iyer A S J, Prudowsky Z and Dickson R M 2010 *J. Phys. Chem. Lett.* **1** 2524
- [33] O'Neill P R, Young K, Schiffels D and Fyngenson D K 2012 *Nano Lett.* **12** 5464
- [34] Muhammed M A H, Aldeek F, Palui G, Trapiella-Alfonso L and Mattoussi H 2012 *ACS Nano* **6** 8950
- [35] Zhang H, Huang X, Li L, Zhang G W, Hussain I, Li Z and Tan B N 2012 *Chem. Commun.* **48** 567
- [36] Yang X, Gan L F, Han L, Wang E K and Wang J 2013 *Angew. Chem. Int. Edn Engl.* **52** 2022
- [37] Kawasaki H, Kosaka Y, Myoujin Y, Narushima T, Yonezawa T and Arakawa R 2011 *Chem. Commun.* **47** 7740
- [38] Chen J H, Liu J, Fang Z Y and Zeng L W 2012 *Chem. Commun.* **48** 1057
- [39] Kawasaki H, Yamamoto H, Fujimori H, Arakawa R, Inada M and Iwasaki Y 2010 *Chem. Commun.* **46** 3759
- [40] Tanaka S I, Miyazaki J, Tiwari D K, Jin T and Inouye Y 2011 *Angew. Chem. Int. Edn Engl.* **50** 431
- [41] Sun H, Sakka Y, Gao H, Miwa Y, Fujii M, Shirahata N, Bai Z and Li J 2011 *J. Mater. Chem.* **21** 4060
- [42] Sun H, Sakka Y, Fujii M, Shirahata N and Gao H 2011 *Opt. Lett.* **36** 100
- [43] Sun H, Sakka Y, Shirahata N, Gao H and Yonezawa T 2012 *J. Mater. Chem.* **22** 12837
- [44] Sun H, Xu B, Yonezawa T, Sakka Y, Shirahata N, Fujii M, Qiu J and Gao H 2012 *Dalton Trans.* **41** 11055
- [45] Sun H, Yonezawa T, Gillett-Kunnath M M, Sakka Y, Shirahata N, Gui S, Fujii M and Sevov S C 2012 *J. Mater. Chem.* **22** 20175
- [46] Grasset F, Molard Y, Cordier S, Dorson F, Mortier M, Perrin C, Guilloux-Viry M, Sasaki T and Haneda H 2008 *Adv. Mater.* **20** 1710
- [47] Aubert T, Nerambourg N, Saito N, Haneda H, Ohashi N, Mortier M, Cordier S and Grasset F 2013 *Part. Syst. Charact.* **30** 90
- [48] Molard Y, Labbé C, Cardin J and Cordier S 2013 *Adv. Funct. Mater.* **23** 4821
- [49] Udayabhaskararao T, Sun Y, Goswami N, Pal S K, Balasubramanian K and Pradeep T 2012 *Angew. Chem. Int. Edn Engl.* **51** 2155
- [50] Mohanty J S, Xavier P L, Chaudhari K, Bootharaju M S, Goswami N, Pal S K and Pradeep T 2012 *Nanoscale* **4** 4255
- [51] Andolina C M, Dewar A C, Smith A M, Marbella L E, Hartmann M J and Millstone J E 2013 *J. Am. Chem. Soc.* **135** 5266
- [52] Yu Y, Yao Q F, Luo Z T, Yuan X, Lee J Y and Xie J P 2013 *Nanoscale* **5** 4606
- [53] Yuan X, Luo Z T, Yu Y, Yao Q F and Xie J P 2013 *Chem. Asian J* **8** 858
- [54] Vajda S *et al* 2009 *Nature Mater.* **8** 213
- [55] Wu Z K and Jin R C 2010 *Nano Lett.* **10** 2568
- [56] Hughbanks T and Hoffmann R 1983 *J. Am. Chem. Soc.* **105** 1150
- [57] Saito T and Imoto H 1996 *Bull. Chem. Soc. Japan* **69** 2403
- [58] Brosset C 1945 *Ark. Kemi. Mineral. Geol.* **20A** 1
- [59] Vaughan P A 1950 *Proc. Natl Acad. Sci. USA* **36** 461
- [60] Maverick A W and Gray H B 1981 *J. Am. Chem. Soc.* **103** 1298

- [61] Maverick A W, Najdzionek J S, MacKenzie D, Nocera D G and Gray H B 1983 *J. Am. Chem. Soc.* **105** 1878
- [62] Davis H L, Bjerrum N J and Smith J P 1967 *Inorg. Chem.* **6** 1172
- [63] Bjerrum N J and Smith J P 1967 *Inorg. Chem.* **6** 1968
- [64] Bjerrum N J, Davis H L and Smith J P 1967 *Inorg. Chem.* **6** 1603
- [65] Bjerrum N J, Boston C R and Smith J P 1967 *Inorg. Chem.* **6** 1162
- [66] Boston C R and Smith G P 1962 *J. Phys. Chem.* **66** 1178
- [67] Boston C R, Smith G P and Howick L C 1963 *J. Phys. Chem.* **67** 1849
- [68] Ruck M 2001 *Angew. Chem. Int. Edn Engl.* **40** 1182
- [69] Ruck M 1997 *Angew. Chem. Int. Edn Engl.* **36** 1971
- [70] Ruck M 1998 *Z. Anorg. Allg. Chem.* **624** 521
- [71] Ruck M and Hampel S 2002 *Polyhedron* **21** 651
- [72] Ruck M, Dubenskyy V and Söhnle T 2003 *Angew. Chem. Int. Edn Engl.* **42** 2978
- [73] Dubenskyy V and Ruck M 2004 *Z. Anorg. Allg. Chem.* **630** 2458
- [74] Wahl B, Kloo L and Ruck M 2008 *Angew. Chem. Int. Edn Engl.* **47** 3932
- [75] Ahmed E, Köhler D and Ruck M 2009 *Z. Anorg. Allg. Chem.* **635** 297
- [76] Beck J, Brendel C, Bengtsson-Kloo L, Krebs B, Mmmert M, Stankowski A and Ulvenlund S 1996 *Chem. Ber.* **129** 1219
- [77] Sun H T, Sakka Y, Shirahata N, Matsushita Y, Deguchi K and Shimizu T 2013 *J. Phys. Chem. C* **117** 6399
- [78] Frangioni J V 2003 *Curr. Opin. Chem. Biol.* **7** 626
- [79] Sun H *et al* 2011 *Small* **7** 199
- [80] Gao X H, Cui Y, Levenson R M, Chung L and Nie S M 2004 *Nature Biotechnol.* **22** 969
- [81] Holmes P, James K A F and Levy L S 2009 *Sci. Total Environ.* **408** 171
- [82] Xie J P, Zheng Y G and Ying J Y 2010 *Chem. Commun.* **46** 961
- [83] Araki S, Sato H, Yokoyama K and Murata K 2000 *Am. J. Ind. Med.* **37** 193
- [84] Needleman H 2004 *Annu. Rev. Med.* **55** 209
- [85] Yuan Z Q, Peng M H, He Y and Yeung E S 2011 *Chem. Commun.* **47** 11981